

Micro-fabricated stylus ion trap

Christian L. Arrington, Kyle S. McKay, Ehren D. Baca, Jonathan J. Coleman, Yves Colombe, Patrick Finnegan, Dustin A. Hite, Andrew E. Hollowell, Robert Jördens, John D. Jost, Dietrich Leibfried, Adam M. Rowen, Ulrich Warring, Martin Weides, Andrew C. Wilson, David J. Wineland, and David P. Pappas

Citation: *Review of Scientific Instruments* **84**, 085001 (2013); doi: 10.1063/1.4817304

View online: <http://dx.doi.org/10.1063/1.4817304>

View Table of Contents: <http://scitation.aip.org/content/aip/journal/rsi/84/8?ver=pdfcov>

Published by the [AIP Publishing](#)

GRANVILLE-PHILLIPS®

ADVANCED VACUUM MEASUREMENT SOLUTIONS

Vacuum Gauges:

Convectron®, Micro-Ion®, Stabil-Ion®,
Cold Cathode

Mass Spectrometers:

Vacuum Quality Monitors



www.brooks.com

Introducing the First
Cold Cathode Gauge
worthy of the
Granville-Phillips name!

- Unsurpassed Accuracy
- Predictive & Easy Maintenance



Micro-fabricated stylus ion trap

Christian L. Arrington,^{1,a),b)} Kyle S. McKay,^{2,a),c)} Ehren D. Baca,¹ Jonathan J. Coleman,¹ Yves Colombe,² Patrick Finnegan,¹ Dustin A. Hite,² Andrew E. Hollowell,¹ Robert Jördens,² John D. Jost,^{2,d)} Dietrich Leibfried,² Adam M. Rowen,¹ Ulrich Warring,^{2,e)} Martin Weides,^{2,f)} Andrew C. Wilson,² David J. Wineland,² and David P. Pappas²

¹Sandia National Laboratories, Albuquerque, New Mexico 87123, USA

²National Institute of Standards and Technology, Boulder, Colorado 80305, USA

(Received 10 May 2013; accepted 17 July 2013; published online 7 August 2013)

An electroformed, three-dimensional stylus Paul trap was designed to confine a single atomic ion for use as a sensor to probe the electric-field noise of proximate surfaces. The trap was microfabricated with the UV-LIGA technique to reduce the distance of the ion from the surface of interest. We detail the fabrication process used to produce a 150 μm tall stylus trap with feature sizes of 40 μm . We confined single, laser-cooled, $^{25}\text{Mg}^+$ ions with lifetimes greater than 2 h above the stylus trap in an ultra-high-vacuum environment. After cooling a motional mode of the ion at 4 MHz close to its ground state ($\langle n \rangle = 0.34 \pm 0.07$), the heating rate of the trap was measured with Raman sideband spectroscopy to be 387 ± 15 quanta/s at an ion height of 62 μm above the stylus electrodes.

© 2013 AIP Publishing LLC. [<http://dx.doi.org/10.1063/1.4817304>]

I. INTRODUCTION

Anomalous motional heating of trapped ions is a potential roadblock in the development of ion traps for quantum information processing.^{1–6} This heating is typically attributed to electric-field noise from the surfaces of trap electrodes in excess of resistive Johnson noise.^{2,3} It has been observed that the noise can be reduced significantly by cooling the traps to cryogenic temperatures.^{3–5} More recently, comparable reductions of the electric-field noise have been obtained from traps at room temperature using surface cleaning of Au electrodes with *in situ* ion bombardment.⁶ This indicates that the materials and nano-scale processes at the surface of the trap are important. However, progress in studying various materials and/or surface treatments to improve performance is stymied by the long turn-around times required to design, fabricate, assemble, and conduct heating-rate measurements on traps made of different materials and using different processing methods. Recent work by Maiwald *et al.*,⁷ suggests a different route to measure electric-field noise from various materials' surfaces, i.e., by using a three-dimensional “stylus” trap that allows enhanced optical and spatial access to the ion. With this configuration, different surfaces can be prepared and brought into close proximity to an ion that is held above the center trap electrode. The change in the heating rate of the ion

can be measured to determine the electric-field noise added by the surface.

To achieve a proximity that is relevant to ions used for quantum information, i.e., an ion distance, $h \lesssim 100 \mu\text{m}$, from the surfaces, the trap should have features on this scale. In order to fabricate a stylus trap with features of $\lesssim 100 \mu\text{m}$, we utilized UV-LIGA (a German acronym for lithography, electroplating, and molding) technology,^{8–12} i.e., UV photolithography with a thick resist and subsequent metal electroforming with the use of electrodeposition. Using this technique, we have fabricated traps that consist of 150 μm tall structures (see Figs. 1–3). The wafer design is shown in Fig. 1 where the lighter shading represents the first layer (2.5 μm thick) and the darker shading represents the protruding trap features (150 μm thick). The base trap design includes an isolated center post electrode with a separate split ring around it for the RF potential. Four separate posts are located symmetrically outside the RF electrodes for compensation of stray electric fields and for tuning of the trapping potential.

II. FABRICATION

The die used in this work is designed with the stylus close to one edge. The primary advantage of this design is a larger solid angle for light collection (when imaged from the side) compared to some of the dies designed with the stylus located in the center. Other design features that were included on the die used in this work, shown in Fig. 1(b), are a split ground plane to allow for microwave currents along either side of the trap to drive hyperfine transitions in the ion, and a 200- μm -wide wall that shields the gaps between the traces and ground from shorting due to the atomic Mg flux used to load the trap. The wall is fabricated in the same step as the trap features and is shorted to ground. It is built in sections to leave clear areas for laser access.

^{a)}Christian L. Arrington and Kyle S. McKay contributed equally to this work.

^{b)}Electronic mail: clarrin@sandia.gov

^{c)}Electronic mail: kyle.mckay@nist.gov

^{d)}Present address: École Polytechnique Fédérale de Lausanne, 1015 Lausanne, Switzerland.

^{e)}Present address: Albert-Ludwigs-Universität Freiburg, Physikalisches Institut, Freiburg, Germany.

^{f)}Present address: Physikalisches Institut, Karlsruhe Institute of Technology and DFG-Center for Functional Nanostructures (CFN) D-76128 Karlsruhe, Germany.

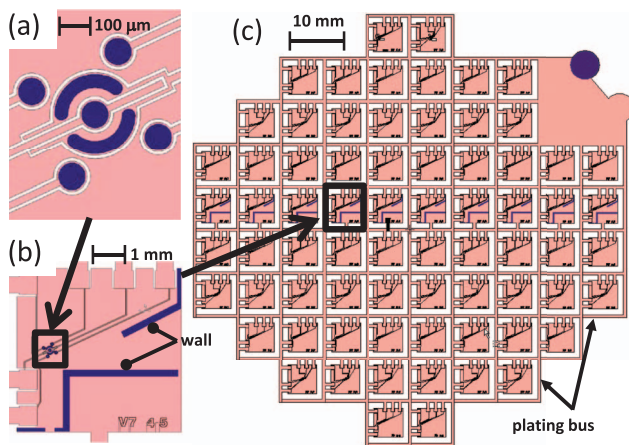


FIG. 1. Layout image showing (a) trap design, (b) individual die level, and (c) the wafer layout. The lightly shaded regions represent the first layer which is used for routing and the darker shaded regions represent the second layer, which are the protruding trap features.

The devices consist of two electroplated layers. The first layer (light shaded regions in Fig. 1) is made of $\sim 2.5 \mu\text{m}$ thick Au. It includes bond pads and traces to the trap that are isolated from the ground plane. The traces are $20 \mu\text{m}$ wide, with gaps to the ground plane of $10 \mu\text{m}$.

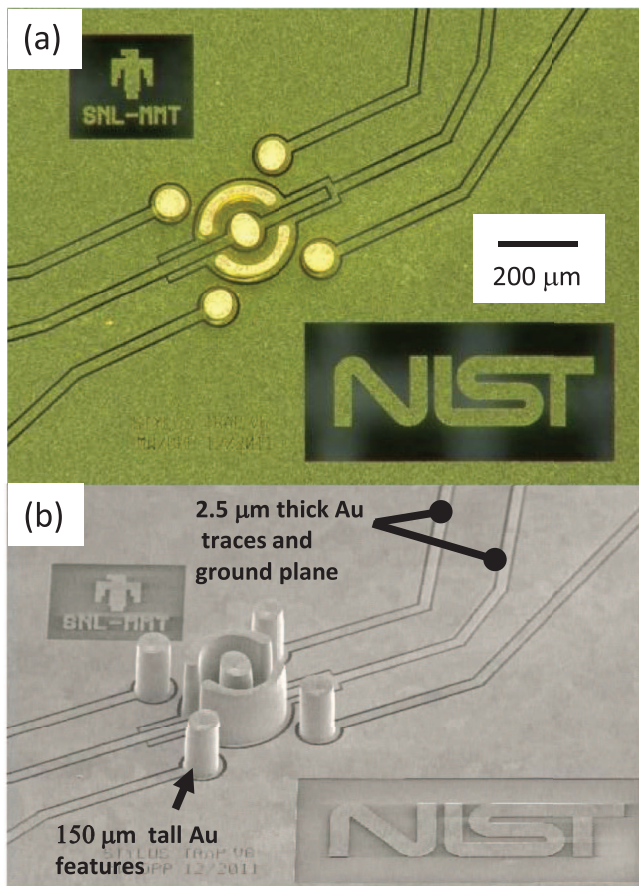


FIG. 2. (a) Optical and (b) scanning electron microscope (SEM) images showing trap features. Each post has electrical connection leads that are connected to bond pads on perimeter of each die. To reduce exposed insulating substrate area, the die used in the experiment did not have the logos.

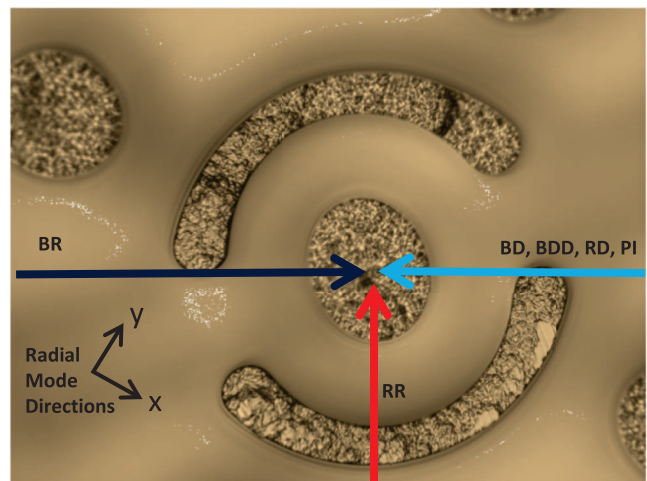


FIG. 3. Optical micrograph of the trap used in the experiments. The paths of the laser beams are overlaid as arrows. The BD, BDD, RD, and PI beams are co-linear and focused at $\sim 60 \mu\text{m}$ above the trap, coming up, out of the plane at an angle of $\sim 4^\circ$ from right to left. The BR and RR beams are parallel to the plane of the trap.

To begin fabrication, a polished, 100-mm-diameter, 0.5-mm-thick fused quartz wafer is cleaned with organic solvents and then coated with a Ti/Au/Ti seed layer (20/100/20 nm) by e-beam evaporation. A layer of AZ 4330¹³ photoresist (2-ethoxyethyl-acetate based positive-tone resist) is then spun at 2000 rpm for 30 s to obtain a thickness of $5.4 \mu\text{m}$. The photoresist is baked on a hotplate for 90 s at 90°C and subsequently exposed with a dose of $258 \text{ mJ}/\text{cm}^2$ UV light (350–400 nm) through a contact mask with the pattern of the first layer. The pattern is then developed using MF 319 [2.2% tetramethylammonium hydroxide (TMAH)] for 2 min, exposing the top Ti seed layer. A 1-min oxygen plasma is used to remove any residual photoresist. Prior to electrodeposition, the top Ti seed layer is removed by submersion of the wafer for 30 s in 100:1 $\text{H}_2\text{O}:\text{HF}$ solution. This exposes the conductive Au seed layer.

Gold electrodeposition is performed using an Enthone 309i gold-sulfite chemistry at 50°C . During deposition, the current is pulsed at 700 Hz with a 25% duty cycle. Before plating the actual wafers, tests were conducted on dummy wafers to determine an optimal current density to achieve uniformity in the heights of the out-of-plane features. An optimal current density of $2 \text{ mA}/\text{cm}^2$ was determined in tests where the applied current was varied and the test wafer was periodically pulled out of the bath. This current density gave a deposition rate of $\sim 5 \mu\text{m}/\text{h}$, so a plating time of 30 min was used for the first layer to achieve a nominal thickness of $2.5 \mu\text{m}$. The photoresist mold is removed using a 1-min acetone soak, and the wafer is then rinsed with isopropanol and dried with N_2 . An Ar-ion mill is performed to anisotropically etch through the conductive seed layer, thereby electrically isolating the traces and ground plane at the die level.

The trap features are defined in the second layer by use of UV-LIGA to electrodeposit a thick Au film. This process determines the minimum feature size, hence the maximum aspect ratio. Preliminary tests showed that features $150 \mu\text{m}$ tall with lateral dimensions $\sim 40 \mu\text{m}$ gave acceptable yields.

A conservative implementation of this design rule was used throughout. More specifically, in this design the posts are nominally 80 μm in diameter, the RF electrodes are 40 μm wide, and the gaps between the posts and the RF electrodes are 40 μm . The features in the second layer are designed to leave a 5- μm -wide margin in the first layer to allow for slight misalignment of the layers.

For the second-layer electrodeposition, the dies are surrounded at the wafer level by a grid of bus bars [see Fig. 1(c)] that carry plating current. Connections are made between the bus-bar grid to each of the traces for the trap features and to the lower ground plane for the wall [see Fig. 1(b)]. To define the trap and wall, a thick photoresist layer is spun on the wafer and patterned to create a mold. This photoresist layer is typically $\sim 10\ \mu\text{m}$ thicker than the height of the features, i.e., $\sim 160\ \mu\text{m}$. To accomplish this, KMPR 1050 (epoxy-based negative-tone photoresist) is spun onto the wafer at 1200 rpm for 10 s.^{10,11} The wafer is then baked at 100 °C on a hot plate for 2 h and left in ambient conditions for 12 h to allow the solvents to out-gas from the resist. The wafer is baked again on the hotplate at 100 °C for 15 min to further drive out residual solvent. If any wrinkling of the resist is observed during the bake, then after the bake the wafer is left at room temperature for 2 h to allow for additional outgassing. This cycle of baking/out-gassing/baking is repeated until the photoresist does not wrinkle during the bake, indicating that enough of the solvent has been removed to continue the process. Typically, from the short spin step, there is a thick bead of photoresist around the edge of the wafer. If so, this bead is removed with a sharp edge to leave a planar surface. This allows for more uniform contact of the photo-mask during the subsequent UV light exposure. For this exposure, a dose of 1350 mJ/cm² is used. Post-exposure bakes at 100 °C for 4.5 min and then 65 °C for 1 min are then performed. The unexposed KMPR is developed away using NMD-W (2.38% TMAH), and an oxygen plasma is used to remove any residual photoresist at the bottom of the developed features.

The second Au layer is deposited using the same chemistry as the first; however, the deposition time is significantly longer ($\sim 30\ \text{h}$) in order to grow 150 μm structures. The individual 5 \times 5 mm² dies are then cut out from the wafer as close as possible to the ground plane in order to minimize the area of exposed insulating substrate. This reduces uncontrolled potentials from charging effects when trapping ions. During the dicing process, the wafer is mounted to a stainless-steel ring with adhesive dicing tape. Because of the nature of the ion-trap design, i.e., with tall Au posts that can be easily deformed by the pressure of a mounting system roller, the dicing tape is first applied to the stainless-steel ring. The wafer is then mounted onto the tape. The stainless-steel ring provides support for the wafer and mechanically locks into the dicing saw. Dicing is performed using a 0.25-mm-thick, 45- μm -grit resinoid blade. The saw is operated at a spindle spin speed of 14 000 rpm with a forward cut speed of 1.27 mm/s. During dicing, the photoresist is left intact to protect the devices. To remove the photoresist after dicing, the dies are first submerged into a NMP (1-methyl-2-pyrrolidone) based solvent at 80 °C for 25 min with 100-rpm stir-bar agitation. This delaminates the photoresist films from the first

layer; however, the photoresist still remains attached to the trap features. The dies are then rinsed with DI water and immersed into a 3:1 H₂SO₄:H₂O₂ solution for 3 min to release the photoresist from the trap features. The result is shown in Fig. 2. Quality inspection of the dies is performed by use of an electrical probe station and an optical microscope.

Two wafers were run through the above process, with about 40% of dies passing visual and electrical testing. Of the bad dies, about 20% of the total failed the electrical-isolation-to-ground test (i.e., a first-layer failure), and 40% had over-plated some areas of the mold during the second layer deposition. The yield of the process could be improved by adding a planarization step after the second layer deposition to remove the over-plated Au. In the dies that passed inspection, however, the trap features are slightly distorted relative to the design, as is evident in Fig. 3. More specifically, the center post-electrode tends to be compressed in the direction along the split in the RF electrode, while the RF electrodes have enlarged ends and are narrowed in the center. The four posts around the outside are also elongated along the directions pointing towards the RF electrodes. The alignment of these deformations indicates that it is caused by swelling of the photoresist during the processing, with less swelling occurring in the gaps between the electrodes.⁹ The swelling of the resist is a result of exposure to the high alkaline (Na based) plating baths, particularly at an elevated temperature (50 °C). Swelling also resulted from an increased solvent concentration in the thick resist. Compared to the same resist with a smaller thickness, a higher solvent concentration was necessary for proper development of the resist. After developing the resist, additional baking helps reduce the solvent concentration and decrease swelling of the resist.

III. OPERATION

The trap is mounted inside an ultra-high-vacuum chamber ($< 2 \times 10^{-8}\ \text{Pa}$). A photograph of the chip is shown in Fig. 4. The chip is mounted on a pedestal to allow for access of the lasers without obstruction from the assembly, e.g., the bond wires and *in situ* components. The bond pads around

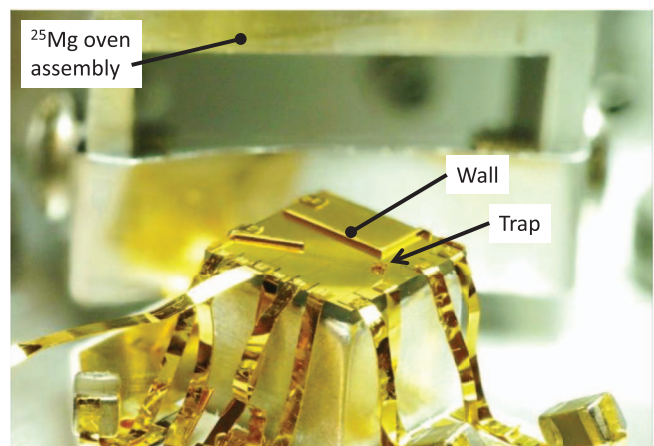


FIG. 4. Stylus-trap chip mounted in the vacuum chamber. One of the five compensation-post filter capacitors can be seen at the bottom right. The ²⁵Mg evaporator is in the background.

the perimeter of the die are gap-welded to a circuit board for electrical contacts, with 3.5 nF capacitors and 10 k Ω resistors that form resistor-capacitor (RC) low-pass filters between the external lines and the five posts. The RF electrodes are connected to a helical resonator that is external to the vacuum system. The entire circuit, i.e., helical resonator, feedthrough, and trap, is resonant at 62.2 MHz. Power is applied to the circuit to obtain a nominal voltage at the trap of 85 V. The five posts are connected to DC sources, and the voltages are adjusted in order to control the asymmetry of the trapping potential and to minimize micromotion of the ion in the trap.¹⁴ The trap geometry was analyzed using boundary element method simulations,^{15–17} which predict an ion height of 62 μm above the center trap electrode. For a trap voltage of 85 V, the simulations predict a pseudopotential trap depth of ~ 100 meV, radial-mode (in-plane) frequencies of ~ 4 MHz and an axial (out-of-plane) frequency of ~ 8 MHz. Additional DC voltages were added to the posts to define the directions of and to reduce the degeneracy of the radial-mode frequencies. The measured radial frequencies for the x and y directions were 3.7 MHz and 4.0 MHz, respectively (see Fig. 3). The oven, shown in the back of Fig. 4, supplies a flux of ^{25}Mg neutral atoms from an evaporation source to the trapping region. The wall on the chip is positioned so as to protect the gaps between traces and ground from the ^{25}Mg flux.

The $^{25}\text{Mg}^+$ ion was chosen to ease the requirements of the laser system. Using a scheme similar to Epstein *et al.*,¹⁸ the required Doppler and Raman cooling lasers were derived from a single 279.67-nm source (a frequency quadrupled fiber laser at 1118 nm). As shown in Fig. 5, six double-pass acousto-optic modulators (AOMs) were used to generate five beams for cooling and detection of the ion.

Figure 6 shows a simplified level diagram of $^{25}\text{Mg}^+$ in a magnetic field of 1.0 mT. The transition between the $|F=3,$

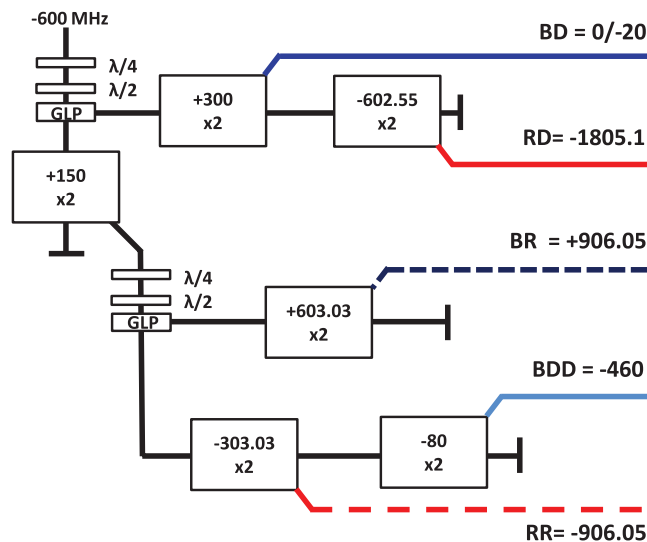


FIG. 5. Acousto-optic modulator setup used to generate the five Doppler and Raman cooling lasers for $^{25}\text{Mg}^+$ from a single 279.67-nm source. The input -600 MHz (upper left) and output detunings (right) are referenced to the $^2\text{S}_{1/2} |3, -3\rangle$ to $^2\text{P}_{3/2} |4, -4\rangle$ transition. All detunings and AOM frequency shifts have units of MHz. GLP: Glan-laser prism

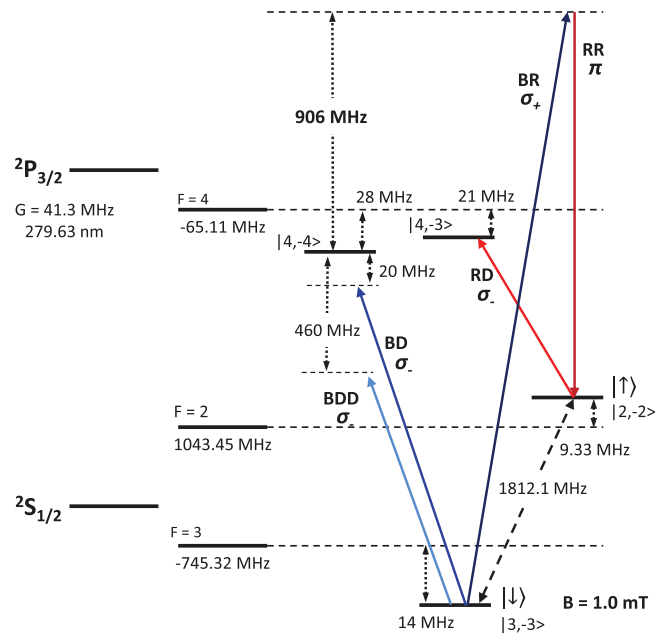


FIG. 6. Simplified level diagram of $^{25}\text{Mg}^+$. The left column shows the electronic levels without hyperfine structure. The next column shows the energy levels including hyperfine structure, at zero magnetic field. The right side of the figure shows the relevant Zeeman sublevels in a magnetic field of 1.0 mT. Solid arrows represent transitions addressed with lasers, while dashed arrows represent microwave-addressed transitions. Dotted arrows represent frequency separations. The nominal polarizations of the laser beams are indicated with the beam labels.

$m_F = -3$) state of the $^2\text{S}_{1/2}$ manifold and the $|4, -4\rangle$ state of the $^2\text{P}_{3/2}$ manifold, which has an excited state linewidth of 41.3 MHz, was selected as the Doppler cooling transition. The blue Doppler cooling beam (BD, σ_- polarized) is red detuned from the cooling transition by 20 MHz during cooling and red detuned by ~ 4 MHz during detection. The detuned blue Doppler cooling beam (BDD, σ_- polarized) is red detuned by 460 MHz and is used to cool hot ions, particularly when loading. During Doppler cooling, the ion has some probability of decaying into the $F = 2$ ground state due to imperfect polarization of the BD and BDD beams; therefore, the red Doppler beam (RD, σ_- polarized) is used to repump the ion back to the $F = 3$ ground state.

The BD, BDD, and RD beams, along with a photoionization beam (285 nm), are combined using 50/50 beam splitters and a Glan-laser prism. The combined, collinear beam is focused ~ 60 μm above the trap and propagates at an angle with respect to all of the motional modes of the trap (see Fig. 3).¹⁹ The ion is imaged from above (as in the view of Fig. 3) using a F 1.4 lens assembly onto either a photomultiplier tube (PMT) or an electron-multiplying-charge-coupled-device (EMCCD) camera (selected using a flipper mirror). The ion can also be imaged from the side with a reentrant viewport and a F 1.6 lens assembly.

The blue Raman (BR, σ_+ polarized) and red Raman (RR, π polarized) beams are used to excite Raman transitions, which enable cooling to near the ground state of the motion.²⁰ When the relative detuning of the RR and BR beams are set to 1812.1 MHz, the ion undergoes a carrier transition from the $|3, -3\rangle$ state ($|\downarrow\rangle$) to the $|2, -2\rangle$ state ($|\uparrow\rangle$) where the mo-

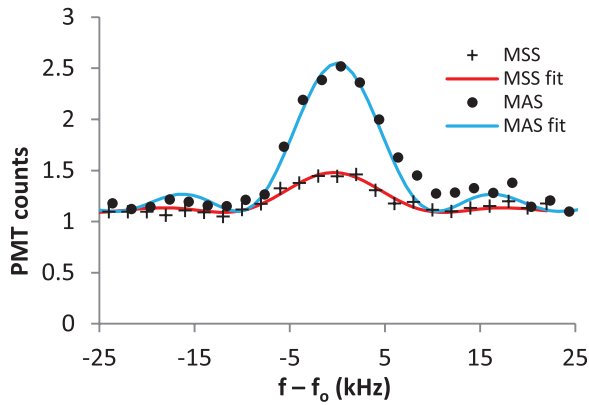


FIG. 7. Frequency sweep of the BR laser to show the sidebands for the MSS and MAS transitions after 45 cycles of Raman cooling. The fitted sideband amplitudes²¹ indicate that the ion is cooled to an average motional quanta of $\langle n \rangle = 0.34 \pm 0.07$. The frequencies of the sidebands are shifted so that the curves overlap. The background of the sidebands is large because of the high spontaneous emission rates from the relatively small Raman detunings.¹⁸

tional state remains unchanged. By reducing the relative detuning by a mode frequency of the trap, a single quantum of energy can be removed from the ion's motional mode. This is referred to as a motion-subtracting-sideband (MSS) transition. Similarly, by increasing the relative detuning by a mode frequency, a quantum of energy is added, which is referred to as a motion-adding-sideband (MAS) transition. The motional energy of the ion can be determined by measuring the ratio of the MAS and MSS transition amplitudes² (see Fig. 7). The ratio of the MAS and MSS transition amplitudes ($R = \text{amp. of MSS}/\text{amp. of MAS}$) can be used to determine the average motional quantum number for the mode being cooled $\langle n \rangle = R/(1 - R)$.

The heating rate of the stylus trap was measured by first cooling the ion with Doppler cooling to near the Doppler limit. Then, 45 Raman cooling cycles were applied to cool the y radial-frequency mode of the ion down to near the ground state to an average motional quantum number, $\langle n_y \rangle$, of 0.34 ± 0.07 . A cooling cycle consists of a MSS pulse to remove a quantum of energy, followed by a RD pulse to reinitialize the ion to the $|\downarrow\rangle$ state. After completing all cooling cycles, the cooling lasers were switched off and the ion was

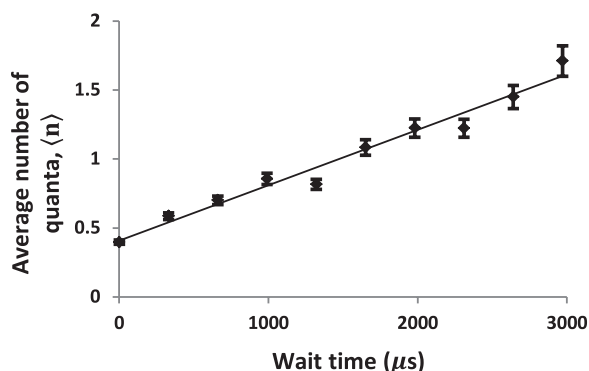


FIG. 8. Plot of the average motional quanta as a function of wait time after applying 45 cycles of Raman cooling. The heating rate of 387 ± 15 quanta/s was measured at a mode frequency of 4 MHz and an ion height of $62 \mu\text{m}$.

allowed to heat for durations up to 3 ms, after which the amplitude of either the MAS or the MSS Raman sideband of the ion was measured to determine the average motional energy of the mode being cooled as described above. From the dependence of the average motional energy on the wait time, a heating rate of 387 ± 15 quanta/s was observed for an ion height of $62 \mu\text{m}$ and a mode frequency of 4 MHz (see Fig. 8). The measured heating rate corresponds to an electric-field-noise spectral density of $6.7 \times 10^{-12} \text{ V}^2 \text{ m}^{-2} \text{ Hz}^{-1}$, which is comparable with heating rates of other room-temperature surface-electrode traps.⁶

IV. CONCLUSION

We have developed and demonstrated the viability of batch-fabricated, electroformed, stylus ion traps. The fabricated devices should enable single-ion trapping experiments to better characterize and reduce ion heating, with an ultimate goal of contributing to future quantum information technology. The UV-LIGA fabrication process is not limited to the fabrication of stylus traps and is useful for fabrication of other devices with thick metal features.

Magnesium was chosen for this work, but the device could be utilized for other ion species by adjusting trapping conditions accordingly. At a distance of $62 \mu\text{m}$ to the closest electrode surface, the heating rate of the trap was measured to be 387 ± 15 quanta/s for a radial mode frequency of 4 MHz. Future work will include the addition of an XYZ manipulator to position test surfaces into close proximity of the ion so that the added electric-field noise of test surfaces as a function of their distance to the ion can be studied.

ACKNOWLEDGMENTS

This work was supported by IARPA under ARO Contract No. DNI-017389, ONR, and the NIST Quantum Information program.

¹D. J. Wineland, C. Monroe, W. M. Itano, D. Leibfried, B. E. King, and D. M. Meekhof, *J. Res. Natl. Inst. Stand. Technol.* **103**, 259 (1998).

²Q. A. Turchette, Kielpinski, B. E. King, D. Leibfried, D. M. Meekhof, C. J. Myatt, M. A. Rowe, C. A. Sackett, C. S. Wood, W. M. Itano, C. Monroe, and D. J. Wineland, *Phys. Rev. A* **61**, 063418 (2000).

³L. Deslauriers, S. Olmschenk, D. Stick, W. K. Hensinger, J. Sterk, and C. Monroe, *Phys. Rev. Lett.* **97**, 103007 (2006).

⁴J. Labaziewicz, Y. Ge, D. R. Leibbrandt, S. X. Wang, R. Shewmon, and I. L. Chuang, *Phys. Rev. Lett.* **101**, 180602 (2008).

⁵S. X. Wang, Y. Ge, J. Labaziewicz, E. Dauler, K. Berggren, and I. L. Chuang, *Appl. Phys. Lett.* **97**, 244102 (2010).

⁶D. A. Hite, Y. Colombe, A. C. Wilson, K. R. Brown, U. Warring, R. Jördens, J. D. Jost, K. S. McKay, D. P. Pappas, D. Leibfried, and D. J. Wineland, *Phys. Rev. Lett.* **109**, 103001 (2012).

⁷R. Maiwald, D. Leibfried, J. Britton, J. C. Bergquist, G. Leuchs, and D. J. Wineland, *Nat. Phys.* **5**, 551 (2009).

⁸E. W. Becker, W. Ehrfeld, D. Münchmeyer, H. Betz, A. Heuberger, S. Pongratz, W. Glashauser, H. J. Michel, and R. v. Siemens, *Naturwiss.* **69**, 520 (1982).

⁹L. Yi, W. Xiaodong, L. Chong, L. Zhifeng, C. Denan, and Y. Dehui, *Microsyst. Technol.* **11**, 1272 (2005).

¹⁰C. H. Lee and K. Jiang, *J. Micromech. Microeng.* **18**, 055032 (2008).

¹¹Y.-M. Shin, D. Gamzina, L. Barnett, F. Yaghmaie, A. Baig, and N. Luhmann, *J. Microelectromech. Syst.* **19**, 683 (2010).

¹²J. D. Williams and W. Wang, *Microsyst. Technol.* **10**, 699 (2004).

¹³Certain commercial equipment, instruments, or materials are identified in this paper to foster understanding. Such identification does

- not imply recommendation or endorsement by the National Institute of Standards and Technology, nor does it imply that the materials or equipment identified are necessarily the best available for the purpose.
- ¹⁴D. J. Berkeland, J. D. Miller, J. C. Bergquist, W. M. Itano, and D. J. Wineland, *J. Appl. Phys.* **83**, 5025 (1998).
- ¹⁵BEM Package developed by NIST Ion Storage Group based on FastLap, a numerical solver package from the RLE Computational Prototyping Group at MIT.
- ¹⁶T. Korschmeier, K. Nabors, and J. White, *FastLap2.0*, Massachusetts Institute of Technology, Cambridge, MA, 1996.
- ¹⁷K. Nabors, T. Korschmeier, F. Leighton, and J. White, *SIAM J. Sci. Comput.* **15**, 713 (1994).
- ¹⁸R. J. Epstein, S. Seidelin, D. Leibfried, J. H. Wesenberg, J. J. Bollinger, J. M. Amini, R. B. Blakestad, J. Britton, J. P. Home, W. M. Itano, J. D. Jost, E. Knill, C. Langer, R. Ozeri, N. Shiga, and D. J. Wineland, *Phys. Rev. A* **76**, 033411 (2007).
- ¹⁹W. M. Itano and D. J. Wineland, *Phys. Rev. A* **25**, 35 (1982).
- ²⁰F. Diedrich, J. C. Bergquist, W. M. Itano, and D. J. Wineland, *Phys. Rev. Lett.* **62**, 403 (1989).
- ²¹H. J. Metcalf and P. van der Straten, *Laser Cooling and Trapping* (Springer, 1999).